LAWRENCE
LIVERMORE
NATIONAL
LABORATORY

LLNL-JRNL-561593

Comparison of spectral line Stark broadening models

C. Iglesias

June 18, 2012

High energy density physics

Disclaimer

Comparison of spectral line stochastic Stark broadening models

CARLOS A. IGLESIAS
Lawrence Livermore National Laboratories
P.O. Box 808, Livermore, CA 94550, USA

Abstract

Spectral line stochastic Stark broadening models are applied to the Lyman-α line of hydrogenic ions resulting in relatively simple expressions for the profile. Furthermore, the profiles yield analytic formulas for known limits of the general spectral line broadening theory; thus, it is possible to identify limitations of the stochastic models.

Keywords:
Stark broadening, spectral lines, ion dynamics, quasi-static limit, impact limit

Corresponding author:
e-mail: iglesias1@llnl.gov (C. A. Iglesias)

1. Introduction

It is well established that the quasi-static ion approximation in spectral line Stark broadening calculations can lead to discrepancies with experimental data near line center [1]. A successful and practical approach to incorporate particle dynamics is a stochastic model microfield description of the plasma [2,3] (respectively MMM and BID hereafter). These models obtain exact solutions for the line profile assuming an idealized stochastic process and conserve important properties of the real problem by adjusting free parameters present in the theory.

A related approach is the frequency-fluctuation model (FFM) [4]. This model assumes a Markovian process for the fluctuations of the emitted or absorbed radiation. Specifically, the plasma fluctuations cause an exchange between the quasi-static radiative channels. In addition, the FFM permits fast calculations of spectral line profiles for large problems.

The purpose here is to examine the behavior of the FFM and BID formulations when applied to the Lyman-α line of hydrogenic ions. This yields relatively simple expressions for the line profiles and analytic results for known limits of the general spectral line broadening theory. Such comparisons can identify limitations of the stochastic models.

2. Radiator-Plasma System

The system is idealized to simplify the analysis. Hence, the plasma is assumed isotropic and is represented by a single perturbing species. The radiator-perturber interaction assumes the dipole approximation [5] and only internal radiator states with the same principal quantum number are allowed to interact. Finally, it is stressed that there are important differences between neutral and charged radiators [2,3] and the present discussion considers the latter.

The Lyman-α line is the radiative transition from the 2p to 1s orbitals in a one-electron ion where $n\ell$ is the usual notation for principal and orbital quantum numbers. The single lower state plus degenerate upper states (fine structure is neglected) are labeled

$$\begin{aligned} |0\rangle &= |1s, m=0\rangle \\ |1\rangle &= |2s, m=0\rangle \\ |2\rangle &= |2p, m=0\rangle \\ |3\rangle &= |2p, m=+1\rangle \\ |4\rangle &= |2p, m=-1\rangle \end{aligned} \tag{2.1}$$

A vector in ‘line space’ represents the dipole operator for the radiative transitions

$$d = (0,1,1,1)^T \tag{2.2}$$

where the superscript T denotes transpose.

In a coordinate system where the Stark field $\vec{\varepsilon}$ defines the z-axis the only non-zero matrix element of the radiator-perturber interaction is given by

$$\langle 1|\vec{d}\cdot\vec{\varepsilon}|2\rangle = B\varepsilon \tag{2.3}$$

Although B is well known, it is not required after introducing the dimensionless variables

$$\begin{aligned} \beta &= \varepsilon/\varepsilon_o \\ x &= \Delta\omega/B\varepsilon_o \end{aligned} \tag{2.4}$$

where ε_o is a characteristic field strength and $\Delta\omega$ is the photon energy measured from line center. In dimensionless variables,

$$\begin{aligned} d\varepsilon P(\varepsilon) &\to d\beta P(\beta) \\ d\omega L(\Delta\omega) &\to dx L(x) \end{aligned} \tag{2.5}$$

where $P(\varepsilon)$ is the probability of finding an electric field magnitude ε at the radiator due to the plasma and $L(\Delta\omega)$ is the line shape function [5]. The dimensionless variables are used hereafter.

3. Static profile

The area normalized Lyman-α line profile in the quasi-static approximation is given by [5]

$$L_{QS}(x) = \left(\pi d^T\cdot d\right)^{-1}\mathrm{Im}\left\langle d^T\cdot R(x;\beta)d\right\rangle_\beta \tag{3.1}$$

where $u^T\cdot v$ denotes a vector dot product in line space and

$$\left\langle f(\beta)\right\rangle_\beta = \int_o^\infty d\beta P(\beta)f(\beta) \tag{3.2}$$

defines an average over the field magnitude. As usual the angle integration was simplified by letting the electric field define the z-axis (see *Appendix A*). The resolvent in the present approximations reduces to the 4x4 matrix [5]

$$R(x;\beta) = \begin{pmatrix} \dfrac{x-i\gamma}{(x-i\gamma)^2-\beta^2} & \dfrac{\beta}{(x-i\gamma)^2-\beta^2} & 0 & 0 \\ \dfrac{\beta}{(x-i\gamma)^2-\beta^2} & \dfrac{x-i\gamma}{(x-i\gamma)^2-\beta^2} & 0 & 0 \\ 0 & 0 & (x-i\gamma)^{-1} & 0 \\ 0 & 0 & 0 & (x-i\gamma)^{-1} \end{pmatrix} \tag{3.3}$$

where γ is a homogenous width assigned to all line components and made to vanish at the end of the calculations. Substituting the transition dipole and resolvent matrix into Eq. (3.1) yields

$$\begin{aligned} L_{QS}(x) &= \frac{1}{3\pi}\left\{\frac{2\gamma}{x^2+\gamma^2} + \mathrm{Im}\left\langle \frac{x-i\gamma}{(x-i\gamma)^2-\beta^2}\right\rangle_\beta\right\} \\ &\underset{\gamma\to 0}{=} \frac{1}{6}\left\{4\delta(x) + P(|x|)\right\} \end{aligned} \tag{3.4}$$

This is a well-known result where the first term is the contribution from the unshifted $m = \pm 1$ states and the second is from the shifted $m = 0$ states.

4. FFM profile

The Lyman-α line profile from FFM that accounts for particle dynamics is given by [4]

$$L_{FFM}(x) = \left(\pi d^T \cdot d\right)^{-1} \mathrm{Im}\left\{d^T \cdot \left[I - i\nu_o \left\langle R(x;\beta)\right\rangle_\beta\right]^{-1} \left\langle R(x;\beta)\right\rangle_\beta d\right\} \tag{4.1}$$

where ν_o is a free parameter and represents the frequency fluctuation rate. Note that $\langle R\rangle_\beta$ appearing in this expression has the Stark field defining the z-axis and the average is over the field magnitude. Since the resolvent has 3 diagonal blocks, the FFM profile has independent contributions from the shifted and unshifted components that are considered separately below.

4.1 Unshifted components, $m = \pm 1$

The profile contribution from the unshifted components is given by

$$\begin{aligned} L_{FFM}^{(|m|=1)}(x) &= \frac{2}{3\pi}\mathrm{Im}\left\{\left(1 - \frac{i\nu_o}{x-i\gamma}\right)^{-1}\left(\frac{1}{x-i\gamma}\right)\right\} \\ &\underset{\gamma\to 0}{=} \frac{2}{3}\left(\frac{\nu_o/\pi}{x^2+\nu_o^2}\right) \end{aligned} \tag{4.1.1}$$

Clearly, the unshifted components simply have their line width modified by the fluctuation rate. Note that in other stochastic models [2,3] the resolvent takes the form $R(x) \to R(x + i\nu_o)$, but not in FFM. This is discussed further in *Appendix B*.

4.2 Shifted components, $m = 0$

The shifted components involve a 2 state system

$$L_{FFM}^{(m=0)}(x) = \frac{1}{3\pi}\mathrm{Im}\left\{\begin{pmatrix}0 & 1\end{pmatrix}\left[\begin{pmatrix}1 & 0\\ 0 & 1\end{pmatrix} - i\nu_o U\right]^{-1} U\begin{pmatrix}0\\ 1\end{pmatrix}\right\}$$
$$= \frac{1}{3\pi}\mathrm{Im}\left\{\frac{U_{11} - i\nu_o\left(U_{11}^2 - U_{12}^2\right)}{\left[1 - i\nu_o\left(U_{11} - U_{12}\right)\right]\left[1 - i\nu_o\left(U_{11} + U_{12}\right)\right]}\right\} \tag{4.2.1}$$

where U is the 2x2 diagonal block resolvent corresponding to the $m = 0$ states in Eq. (3.3) averaged over the field magnitude. Its matrix elements are given by

$$U_{11}(x) = f_o(x) + i\frac{\pi}{2}P(|x|) \tag{4.2.2}$$

$$U_{12}(x) = f_1(x) \pm i\frac{\pi}{2}P(|x|) \quad \begin{cases} x > 0 \\ x < 0 \end{cases} \tag{4.2.3}$$

and

$$f_n(x) = \frac{1}{2}\left\langle\left\{\frac{x-\beta}{(x-\beta)^2 + \gamma^2} \pm \frac{x+\beta}{(x+\beta)^2 + \gamma^2}\right\}\right\rangle_\beta \quad \begin{cases} n = 0 \\ n = 1 \end{cases} \tag{4.2.5}$$

These results are derived in *Appendix C*.

4.3 Limits

The small ν_o limit for the FFM profile is readily obtained from Eqs. (4.1.1), (4.2.1) and (4.2.2) to give

$$\lim_{\nu_o \to 0} L_{FFM}(x) = L_{QS}(x) \tag{4.3.1}$$

and the FFM profile reduces to the static result in Section 3.

It is known that the FFM does not reproduce the impact limit near line center [4]. At line center the large modulation frequency limit of the FFM profile is obtained from Eqs. (4.1.1) and (4.2.1) leading to

$$\lim_{\nu_o \to \infty} L_{FFM}(0) = \frac{1}{\pi\nu_o} \tag{4.3.2}$$

so that the FFM line shape broadens with increasing ν_o. This is not the expected line narrowing behavior associated with the rapid fluctuation limit [4,6].

In the far line wings the FFM profile becomes (see *Appendix C*)

$$\lim_{|x| \to \infty} L_{FFM}(x) = \frac{\nu_o}{\pi x^2} \tag{4.3.3}$$

Clearly, the Lyman-α line FFM profile does not reduce to the quasi-static limit in the far wings. Instead, the FFM profile has an inverse square decay with detuning frequency.

5. BID profile

The BID formulation leads to the Lyman-α line profile [3]

$$L_{BID}(x) = -\left(\pi d^T \cdot d\right)^{-1} \mathrm{Im}\left\{ d^T \cdot \left[1 - i\nu\left\langle M\left(x + i\nu;\vec{\beta}\right)\right\rangle_{\vec{\beta}}\right]^{-1} \left\langle M\left(\omega + i\nu;\vec{\beta}\right)\right\rangle_{\vec{\beta}} d \right\} \tag{5.1}$$

with

$$\nu(x) = \frac{\nu_o}{1 + ix\tau} \tag{5.2}$$

This two-parameter representation preserves the fundamental symmetries resulting from rotation, translation, time reversal, and stationarity. The free parameters ν_o and τ were defined by the low- and high-frequency limits of the momentum auto correlation function. It is stressed that $\langle\cdots\rangle_{\vec{\beta}}$ represents a 3-dimensional average over the field and M is the resolvent operator with the Stark field in an arbitrary direction (see *Appendix A*).

In the no lower state interaction approximation (see *Appendix A*),

$$\begin{aligned} \left\langle M_{\ell m,\ell' m'}\left(x + i\nu;\vec{\beta}\right)\right\rangle_{\vec{\beta}} &= \frac{\delta_{\ell'\ell}\delta_{m'm}}{(2\ell+1)} \sum_{\mu} \left\langle R_{\ell\mu,\ell\mu}\left(x + i\nu;\beta\right)\right\rangle_{\beta} \\ &= \delta_{\ell'\ell}\delta_{m'm} G_{\ell}\left(x + i\nu\right) \end{aligned} \tag{5.3}$$

defining G_ℓ. Substitution of the transition dipole and Eq. (5.3) into Eq. (5.1) yields

$$L_{BID}(x) = -\pi^{-1} \mathrm{Im}\left\{ \frac{G_1(x + i\nu)}{1 - i\nu G_1(x + i\nu)} \right\} \tag{5.4}$$

with

$$G_1(z) = \frac{1}{3}\left\{ \frac{2}{z} + \left\langle \frac{z}{z^2 - \beta^2} \right\rangle_{\beta} \right\} \tag{5.5}$$

obtained from the definition in Eq. (5.3) and Eq. (3.3) with $x \to z$ and $\gamma = 0$.

5.1 Limits

The small ν limit of the BID profile readily follows from Eq. (5.1) together with Eq. (5.5),

$$\begin{aligned} \lim_{\nu \to 0} L_{BID}(x) &= -\pi^{-1} \lim_{\nu \to 0} \mathrm{Im} G_1(x + i\nu) \\ &= L_{QS}(x) \end{aligned} \tag{5.1.1}$$

and reduces to the static result in Section 3.

In the far line wing consider the limit

$$\begin{aligned} \underset{x\tau\to\infty}{Lim}\, L_{BID}(x) &= -\pi^{-1}\,\mathrm{Im}\,G_1(x)\left\{1+\frac{2\nu_o\,\mathrm{Re}\,G_1(x)}{x\tau}\right\} \\ &= L_{QS}(x)+O\left(1/x\tau\right) \end{aligned} \tag{5.1.2}$$

Thus, $L_{BID}(x)$ approaches the static limit in the far wing $\left(|x\tau| >> \nu_o\right)$.

It was previously shown that BID recovers the impact limit near line center for the Lyman-α line [7]. A more general discussion of the impact limit is given in *Appendix D*. In addition, at line center the fast fluctuating limit yields

$$\underset{\nu_o\to\infty}{Lim}\,\mathrm{Re}\,G_1\left(i\nu_o\right) = O(x) \tag{5.1.3}$$

and

$$\underset{\nu_o\to\infty}{Lim}\,\mathrm{Im}\,G_1\left(i\nu_o\right) = -\frac{1}{\nu_o}\left\{1-\frac{\left\langle\beta^2\right\rangle_\beta}{3\nu_o^2}\right\} \tag{5.1.4}$$

Substituting these results into Eq. (5.4) leads to

$$\underset{\nu_o\to\infty}{Lim}\, L_{BID}(0) = \frac{3\nu_o}{\pi\left\langle\beta^2\right\rangle_\beta} \tag{5.1.5}$$

which is the expected line narrowing behavior in the rapid fluctuation limit [6].

6. Numerical results

Numerical results for the Lyman-α profiles from FFM and BID are provided for several ν_o values that graphically display the behavior of the two formalisms. All the profiles are symmetric about line center; thus, only the $x \geq 0$ portions are presented.

6.1 Microfield distribution

The calculations use a microfield distribution of the form [8]

$$P(\beta) = A\frac{\beta^2 e^{-\sqrt{\beta}}}{1+C\beta^{9/2}} \tag{6.1.1}$$

that has the correct functional behavior for the small and large field limits for the field distribution at a charged point. Specifically, the following fit was used

$$\begin{aligned} A &= 2.807 \\ C &= 0.5 \end{aligned} \tag{6.1.1}$$

giving a peak at $\beta \approx 1$ typical of plasma conditions in many applications. Although not strictly necessary the fit simplifies the numerical integrations and is sufficient for the present purpose.

6.2 Line profiles

Profile calculations for the two models are displayed in Figs. 1 and 2 for several values of the free parameter. Since τ is typically small [3,7], the present BID calculations assumed $\tau = 0$, which does not affect the results except in the far wing limit. It follows from the figures that both models approach the static results for small ν_o. For increasing ν_o, however, the FFM does not reproduce the fast fluctuating limit [8]. Instead, the FFM profile becomes broader with increasing ν_o. On the other hand, the BID model does show the expected line narrowing behavior associated with the fast fluctuation limit.

7. Conclusions

Stochastic models of spectral line Stark broadening are reasonably successful in describing particle dynamics [2-4]. Two such models were applied to the Lyman-α line. The resulting profiles yield analytic expressions in several limits that are compared to known results of the general spectral line broadening theory.

It was found that the frequency-fluctuation model (FFM) [4] does not reproduce the impact limit near line center or display the line narrowing associated with the fast fluctuating limit [4,6]. Furthermore, the FFM does not approach the static limit in the far line wing. In fact, in these limits the FFM profile for the Lyman-α line behaves as Lorentzian with width defined by the frequency fluctuation rate. In contrast, the BID model [3] reproduces the impact limit near line center, displays the expected behavior in the rapid fluctuation limit, and reduces to the static profile in the far line wings.

Acknowledgments: This work performed under the auspices of the U.S. Department of Energy by Lawrence Livermore National Laboratory under Contract DE-AC52-07NA27344.

Appendix A: ***Integration over field direction***

The angle average is performed using well-known techniques [9,10]. It is advantageous for the Stark field to define the z-axis; thus, transform the internal radiator states to the chosen frame by a rotation $\Omega(\xi_1,\xi_2,\xi_3)$ parametrized by the Euler angles ξ_1, ξ_2, and ξ_3 [11]. Since the field occurs at random directions, the angle integration is obtained by averaging over all rotations. In the absence of external fields, setting $\xi_1 = \phi$ and $\xi_2 = \theta$, the azimuthal and polar angles of the spherical coordinates respectively, makes ξ_3 arbitrary merely introducing a phase. Hence, the field vectorial integration of the resolvent in double atom notation [5,9,10] is given by

$$\begin{aligned}\int \frac{d\vec{\varepsilon}}{4\pi} P(\varepsilon)\langle\langle \alpha\beta|M|\alpha'\beta'\rangle\rangle &= \int_0^\infty d\varepsilon P(\varepsilon)\left\{\frac{1}{8\pi^2}\int_0^{2\pi} d\xi_3 \int_0^{2\pi} d\phi \int_{-1}^{1} d\cos\theta \langle\langle \alpha\beta|\mathbf{D}^{-1}\mathbf{D}M\mathbf{D}^{-1}\mathbf{D}|\alpha'\beta'\rangle\rangle\right\} \\ &= \sum_{m_1 m_3}\sum_{m_2 m_4}\left\langle R_{am_1bm_3,a'm_2b'm_4}\right\rangle_\varepsilon \left\{\int d\Omega D^{(j_\alpha)*}_{m_1 m_\alpha} D^{(j_\beta)}_{m_3 m_\beta} D^{(j_{\alpha'})}_{m_2 m_{\alpha'}} D^{(j_{\beta'})*}_{m_4 m_{\beta'}}\right\} \\ &= \sum_{jmm'}(2j+1)K^{(jm)}_{\alpha\beta}K^{(jm)}_{\alpha'\beta'}\sum_{m_1 m_3}\sum_{m_2 m_4} K^{(jm')}_{am_1bm_3}\left\langle R_{am_1bm_3,a'm_2b'm_4}\right\rangle_\varepsilon K^{(jm')}_{a'm_2b'm_4}\end{aligned} \tag{A.1}$$

Here, M is the resolvent with the field in arbitrary direction, * denotes complex conjugate, the shorthand notation

$$K^{(jq)}_{\alpha\beta} = (-1)^{j_\alpha - m_\alpha}\begin{pmatrix} j_\alpha & j_\beta & j \\ m_\alpha & -m_\beta & -q\end{pmatrix} \tag{A.2}$$

involving the Wigner 3-j symbol was introduced,

$$R(\omega;\varepsilon) = \mathbf{D}(\Omega)M(\omega;\vec{\varepsilon})\mathbf{D}^{-1}(\Omega) \tag{A.3}$$

is the rotated resolvent operator with z-axis along the Stark field, and

$$\langle f(\varepsilon)\rangle_\varepsilon = \int_o^\infty d\varepsilon\, P(\varepsilon) f(\varepsilon) \tag{A.4}$$

denotes the average over the field magnitude. The radiator internal states are described by $|\alpha\rangle = |\Gamma_\alpha j_\alpha m_\alpha\rangle$ with energy $\hbar\omega_\alpha$, $|\beta\rangle = |\Gamma_\beta j_\beta m_\beta\rangle$ with energy $\hbar\omega_\beta$, and so on, where $|\Gamma jm\rangle$ has total angular momentum j, magnetic quantum number m, and Γ represents any additional quantum numbers necessary to complete the description. In addition, the notation $|\alpha\rangle = |am_\alpha\rangle$ with $a = \Gamma_\alpha j_\alpha$, $|\beta\rangle = |bm_\beta\rangle$ with $b = \Gamma_\beta j_\beta$, was also introduced. The results in Eq. (A.1) also used

$$\begin{aligned}\left\langle\left\langle \alpha\beta\left|\mathbf{D}\right|\alpha'\beta'\right\rangle\right\rangle &= \left\langle\alpha\left|D\right|\alpha'\right\rangle \otimes \left\langle\beta\left|D\right|\beta'\right\rangle^{*} \\ &= \delta_{\Gamma_{\alpha'}\Gamma_{\alpha}}\delta_{j_{\alpha'}j_{\alpha}}\delta_{\Gamma_{\beta'}\Gamma_{\beta}}\delta_{j_{\beta'}j_{\beta}}D^{(j_{\alpha})}_{m_{\alpha}m_{\alpha'}}D^{(j_{\beta})*}_{m_{\beta}m_{\beta'}}\end{aligned} \tag{A.5}$$

with $\otimes$ the direct or Kronecker product,

$$\left\langle\Gamma' j' m'\left|D\right|\Gamma j m\right\rangle = \delta_{\Gamma'\Gamma}\delta_{j'j}D^{(j)}_{m'm} \tag{A.6}$$

plus the symmetry, product, and integration properties of the rotation matrices [11].

A.1 Quasi-static line shape function

The quasi-static line shape function is given by [5]

$$\begin{aligned}I_{QS}(\omega) &= -\pi^{-1}\,\mathrm{Im}\,Tr\left\{\vec{d}\cdot\left\langle M(\omega;\vec{\varepsilon})\right\rangle_{\vec{\varepsilon}}\rho\vec{d}\right\} \\ &= -\pi^{-1}\,\mathrm{Im}\sum_{q}\sum_{\alpha\beta}\sum_{\alpha'\beta'}(-1)^{q}\,d^{(-q)}_{\beta\alpha}\left\langle M_{\alpha\beta,\alpha'\beta'}(\omega;\vec{\varepsilon})\right\rangle_{\vec{\varepsilon}}\rho_{\alpha'}d^{(q)}_{\alpha'\beta'} \\ &= -\pi^{-1}\,\mathrm{Im}\sum_{q}\sum_{\alpha\beta}\sum_{\alpha'\beta'}d^{(q)}_{\alpha\beta}\left\langle R_{\alpha\beta,\alpha'\beta'}(\omega;\varepsilon)\right\rangle_{\varepsilon}\rho_{\alpha'}d^{(q)}_{\alpha'\beta'} \\ &= -\pi^{-1}\,\mathrm{Im}\,Tr\left\{\vec{d}\cdot\left\langle R(\omega;\varepsilon)\right\rangle_{\varepsilon}\rho\vec{d}\right\}\end{aligned} \tag{A.1.1}$$

where Tr denotes a trace over internal radiator states and the density matrix is assumed diagonal with elements ρ_{α} the occupation of state $\left|\alpha\right\rangle$. These results were obtained by using the Winger-Eckart theorem [11] for the q^{th} spherical component of the dipole operator,

$$\begin{aligned}d^{(q)}_{\alpha\beta} &= (-1)^{q}\,d^{(-q)}_{\beta\alpha} \\ &= K^{(1q)}_{\alpha\beta}S^{1/2}_{ab}\end{aligned} \tag{A.1.2}$$

with $S^{1/2}_{ab}$ the reduced matrix element, together with the expression for the vectorial average in Eq. (A.1) and the summation properties of the Wigner 3-j symbols [11]. The last line of Eq. (A.1.1) is the usual starting point for calculations in the quasi-static approximation [5].

A.2 No lower state interaction

A common approximation is to neglect lower state broadening (appropriate for the Lyman-α line). Assuming $\alpha's$ and $\beta's$ represent upper and lower states respectively, then for isotropic plasmas the radiator Hamiltonian is rotationally invariant and independent of the magnetic quantum numbers so that

$$R_{\alpha\beta,\alpha'\beta'} \rightarrow \delta_{\beta'\beta}R^{(b)}_{\alpha\alpha'} \tag{A.2.1}$$

With this approximation the field-averaged resolvent in Eq. (A.1) simplifies to

$$\left\langle M_{\alpha\beta,\alpha'\beta'}(\omega;\vec{\varepsilon})\right\rangle_{\vec{\varepsilon}} \to \delta_{\beta'\beta}\frac{\delta_{j_\alpha j_{\alpha'}}\delta_{m_\alpha m_{\alpha'}}}{(2j_\alpha+1)}\sum_m \left\langle R^{(b)}_{am,a'm}(\omega;\varepsilon)\right\rangle_\varepsilon \tag{A.2.2}$$

reproducing earlier results [3].

Appendix B: ***FFM unshifted components ('incorrect' version)***

Consider $R(x;\beta)\to R(x+i\nu;\beta)$ in Eq. (3.1). Then instead of Eq. (3.1.1) get for the unshifted components,

$$\begin{aligned} L^{(|m|=1)}_{FFM}(x) &\overset{?}{=} \frac{2}{3\pi}\mathrm{Im}\left\{\left(1-\frac{i\nu}{x+i\nu-i\gamma}\right)^{-1}\left(\frac{1}{x+i\nu-i\gamma}\right)\right\} \\ &\underset{\gamma\to 0}{=} \frac{2}{3}\delta(x) \end{aligned} \tag{B.1}$$

and the unshifted components do not experience dynamic effects!

Appendix C: ***The*** U **matrix**

The U matrix is the field averaged block diagonal resolvent for the $m=0$ states in Eq. (3.3),

$$U(x)=\begin{pmatrix} F_o(x) & F_1(x)\\ F_1(x) & F_o(x)\end{pmatrix} \tag{C.1}$$

where

$$F_n(x)=\frac{1}{2}\left\langle \frac{1}{x-i\gamma-\beta}\pm\frac{1}{x-i\gamma+\beta}\right\rangle_\beta \quad \begin{cases} n=0\\ n=1\end{cases} \tag{C.2}$$

Straightforward manipulations give for the imaginary parts

$$\begin{aligned} \mathrm{Im}F_o(x) &= \frac{\gamma}{2}\mathrm{Im}\left\langle \frac{1}{(x-\beta)^2+\gamma^2}+\frac{1}{(x+\beta)^2+\gamma^2}\right\rangle_\beta \\ &\underset{\gamma\to 0}{=} \frac{\pi}{2}P(|x|) \end{aligned} \tag{C.3}$$

and similarly

$$\mathrm{Im}F_1(x)\underset{\gamma\to 0}{=}\pm\frac{\pi}{2}P(|x|) \quad \begin{cases} x>0\\ x<0\end{cases} \tag{C.4}$$

For the real parts get

$$\begin{aligned} \mathrm{Re}F_n(x) &= f_n(x) \\ &= \frac{1}{2}\left\langle \frac{x-\beta}{(x-\beta)^2+\gamma^2}\pm\frac{x+\beta}{(x+\beta)^2+\gamma^2}\right\rangle_\beta \quad \begin{cases} n=0\\ n=1\end{cases} \end{aligned} \tag{C.5}$$

The small and large x limits are readily obtained

$$\underset{x\to 0}{Lim}\, f_n(x) = -\frac{\langle \beta^{2-n} \rangle}{x^{n-1}} \tag{C.6}$$

$$\underset{|x|\to \infty}{Lim}\, f_n(x) = \frac{\langle \beta^{n} \rangle}{x^{n+1}} \tag{C.7}$$

for $n = 0,1$.

Appendix D: ***Impact limit of BID profile***

It is desirable for the stochastic description to recover the impact limit near line center whenever ν is large (fast fluctuations). Begin by writing the BID profile in the general form [3]

$$L_{BID}(\omega) = -\pi^{-1}\,\mathrm{Im}Tr\left\{\vec{d}\cdot\left[I - i\nu(\Delta\omega)\left\langle M(\omega;\vec{\varepsilon})\right\rangle_{\vec{\varepsilon}}\right]^{-1}\left\langle M(\omega;\vec{\varepsilon})\right\rangle_{\vec{\varepsilon}}\rho\vec{d}\right\} \tag{D.1}$$

where Tr denotes a trace over internal radiator states, I is the identity operator, ρ is the density matrix for the radiator-plasma system, and the resolvent is given by

$$M(\omega;\vec{\varepsilon}) = \left\{A(\omega) - L_R(\vec{\varepsilon})\right\}^{-1} \tag{D.2}$$

with

$$A(\omega) = \Delta\omega + i\nu(\omega) \tag{D.3}$$

$$\Delta\omega = \hbar^{-1}[H,\cdots] \tag{D.4}$$

$$L_R(\vec{\varepsilon}) = \hbar^{-1}[\vec{\varepsilon}\cdot\vec{d},\cdots] \tag{D.5}$$

where H is the Hamiltonian for the radiator internal states, $L_R(\vec{\varepsilon})$ is the radiator dipole interaction with the quasi-static Stark field, and $[\cdots,\cdots]$ denotes a commutator.

D.1 Second-order expansion

Near line center the broadening is described by weak interactions and is amenable to perturbation theory. To proceed, the profile in Eq. (D.1) can be rewritten to facilitate an expansion of the denominator in powers of $L_R(\vec{\varepsilon})$,

$$L_{BID}(\omega) = -\pi^{-1}\,\mathrm{Im}Tr\left\{\vec{d}\cdot\left[\left\langle M(\omega;\vec{\varepsilon})\right\rangle_{\vec{\varepsilon}}^{-1} - i\nu(\Delta\omega)I\right]^{-1}\rho\vec{d}\right\} \tag{D.1.1}$$

Using Eqs. (D.2) – (D.5) write (suppressing the ω dependence for clarity)

$$\left\langle M(\vec{\varepsilon})\right\rangle_{\vec{\varepsilon}} = \left\{I + A^{-1}\left\langle L_R(\vec{\varepsilon})A^{-1}L_R(\vec{\varepsilon})\right\rangle_{\vec{\varepsilon}} + \cdots\right\}A^{-1} \tag{D.1.2}$$

The inverse of Eq. (D.1.2) is then given by

$$\left\langle M(\vec{\varepsilon})\right\rangle_{\vec{\varepsilon}}^{-1} = A - \left\langle L_R(\vec{\varepsilon})A^{-1}L_R(\vec{\varepsilon})\right\rangle_{\vec{\varepsilon}} + \cdots \tag{D.1.3}$$

Substituting Eq. (D.1.3) into (D.1.1) yields

$$L_{BID}(\Delta\omega \approx 0) = -\pi^{-1}\,\mathrm{Im}Tr\left\{\vec{d}\cdot\left[\Delta\omega + i\left\langle L_R(\vec{\varepsilon})\nu^{-1}L_R(\vec{\varepsilon})\right\rangle_{\vec{\varepsilon}} + \cdots\right]^{-1}\rho\vec{d}\right\} \tag{D.1.4}$$

in the large ν limit.

Now consider the matrix elements of the second-order expression with ν_o a constant,

$$\left\langle\left\langle\alpha\beta\right|\left\langle L_R(\vec{\varepsilon})\nu_o^{-1}L_R(\vec{\varepsilon})\right\rangle_{\vec{\varepsilon}}\left|\alpha'\beta'\right\rangle\right\rangle = \frac{\left\langle\varepsilon^2\right\rangle_\varepsilon \nu_o^{-1}}{3\hbar^2}\sum_\lambda\left\{\vec{d}_{\alpha\lambda}\cdot\vec{d}_{\lambda\alpha'}\delta_{\beta\beta'} + \delta_{\alpha\alpha'}\vec{d}_{\lambda\beta}\cdot\vec{d}_{\beta'\lambda}\right\} - \vec{d}_{\alpha\alpha'}\cdot\vec{d}_{\beta'\beta} - \vec{d}_{\alpha\alpha'}\cdot\vec{d}_{\beta'\beta}\tag{D.1.5}$$

It is emphasized that the vectorial average plays an important role leading to the results in Eq. (D.1.4). Specifically, the linear term in the Stark field vanish in Eq. (D.1.2) and

$$\left\langle\left(\vec{d}\cdot\vec{\varepsilon}\right)\left(\vec{d}\cdot\vec{\varepsilon}\right)\right\rangle_{\vec{\varepsilon}} = \frac{\left\langle\varepsilon^2\right\rangle_\varepsilon}{3}\vec{d}\cdot\vec{d} \tag{D.1.6}$$

valid for isotropic plasmas.

D.2 Free parameter choice

In earlier work the free parameter was chosen as a scalar of the form [3]

$$\nu(\omega) = \frac{\nu_o}{1 + i\omega\tau} \tag{D.2.1}$$

This two-parameter representation preserves the fundamental symmetries resulting from rotation, translation, time reversal, and stationarity. The free parameters ν_o and τ were defined by the low- and high-frequency limits of the momentum auto correlation function.

Now consider the choice

$$\nu_o^{-1} = -\frac{4nQ^2e^2}{\left\langle\varepsilon^2\right\rangle_\varepsilon}\left[\frac{2\pi}{T}\left(\frac{m_R m_P}{m_R + m_P}\right)\right]^{1/2} iG(\Delta\omega = 0) \tag{D.2.2}$$

where Qe, n, and m_P are the perturber charge, mass, and number density, respectively, m_R is the radiator mass, and T is the plasma temperature in energy units. The complex function $G(\Delta\omega)$ is a thermal average and trace over the perturber wavefunctions. In the dipole approximation $\mathrm{Im}G(\Delta\omega)$ is given by the thermally averaged bremsstrahlung Gaunt factor [12]. Thus, $\mathrm{Im}G(0) = \Lambda$ with Λ the Coulomb logarithm [13]. The choice in Eq. (D.2.2) is therefore an approximation to the diffusion constant [7,14] and consistent with the earlier choice for ν_o [3,7].

The choice in Eq. (D.2.2) leads to

$$\left\langle\left\langle \alpha\beta\middle|\left\langle L_R(\vec{\varepsilon})\nu_o^{-1}L_R(\vec{\varepsilon})\right\rangle_{\vec{\varepsilon}}\middle|\alpha'\beta'\right\rangle\right\rangle \to -\frac{4nQ^2e^2}{3\hbar^2}\left[\frac{2\pi}{T}\left(\frac{m_R m_P}{m_R+m_P}\right)\right]^{1/2}\left\{\delta_{\beta\beta'}\sum_{\alpha''}\vec{d}_{\alpha\alpha''}\cdot\vec{d}_{\alpha''\alpha'}\right.$$
$$\left.+\delta_{\alpha\alpha'}\sum_{\beta''}\vec{d}_{\beta'\beta''}\cdot\vec{d}_{\beta''\beta}-2\vec{d}_{\alpha\alpha'}\cdot\vec{d}_{\beta'\beta}\right\}iG(\Delta\omega=0) \tag{D.2.3}$$

which approximately reproduces the second order-order impact limit [15]. Note that the result in Ref. 15 is for electrons while the expression in Eq. (D.2.3) accounts for arbitrary perturber-radiator reduced mass and perturber charge.

The result in Eq. (D.2.3) does not exactly reproduce the second-order impact limit unless the energy spread of the initial and final level manifolds is less than $\sim\hbar\omega_p$ with

$$\omega_p^2=\frac{4\pi Q^2e^2n}{m_P} \tag{D.2.4}$$

the plasma frequency. That is, $\mathrm{Im}G(\omega)$ is nearly constant for $|\omega|\le\omega_p$ (assumes $\hbar\omega_p << T$ so that the detailed balance correction is negligible [12]). Hence, near line center nearly degenerate initial and final levels yields for the arguments of $G(\omega)$ in the second-order dynamic term [15]

$$G(\omega_{\alpha''}-\omega_\alpha)\approx G(\omega_{\alpha'}-\omega_\alpha)\approx G(\omega_{\beta'}-\omega_\beta)\approx G(\omega_{\beta''}-\omega_\beta)\approx G(0) \tag{D.2.5}$$

in agreement with Eq. (D.2.3). The analysis above also assumes $\Delta\omega\tau << 1$ near line center [3].

References

[1] E. Stambulchik & Y. Maron, *HEDP* **6**, 9(2010); *and references therein*.

[2] A. Brissaud & U.Frisch, *JQSRT* **11**, 1767(1971)

[3] D.B. Boercker, C.A. Iglesias & J.W. Dufty*, Phys.Rev.* **A**36, 2254(1987)

[4] B. Talin *et al*, *Phys.Rev* **A51**, 1918(1995)

[5] H.R. Griem, *Spectral Line Broadening in Plasmas* (Academic Press, New York & London, 1974)

[6] R. Kubo, in *Fluctuation, Relaxation, and Resonance in magnetic Systems*, editor D. ter Haar (Oliver and Boyd, Edinburgh, 1962)

[7] D.B. Boercker, in *Spectral Line Shapes Vol. 5*, ed. J. Szudy (Ossolineum, Warszawa, 1989)

[8] A.Y. Potekhin, G. Chabrier & D. Gilles, *Phys.Rev*. **E65**, 036412(2002)

[9] M. Baranger, *Phys.Rev* **111**, 494(1958)

[10] J. Cooper, *Rev.Mod.Phys*. **39**,167(1967)

[11] A.R Edmonds, *Angular Momentum in Quantum Mechanics* (Princeton University Press, Princeton, NJ, 1960)

[12] J.T. O'Brien & C.F. Hooper, *JQSRT* **14**, 479(1974)

[13] G. Bekefi, *Radiation Processes in Plasmas* (John Wiley & Sons, New York, 1966)

[14] D.B. Boercker & E.L. Pollock, *Phys.Rev*. **A36**, 1779(1987)

[15] L.A. Woltz & C.F. Hooper, *Phys.Rev*. **38**, 4766(1988)

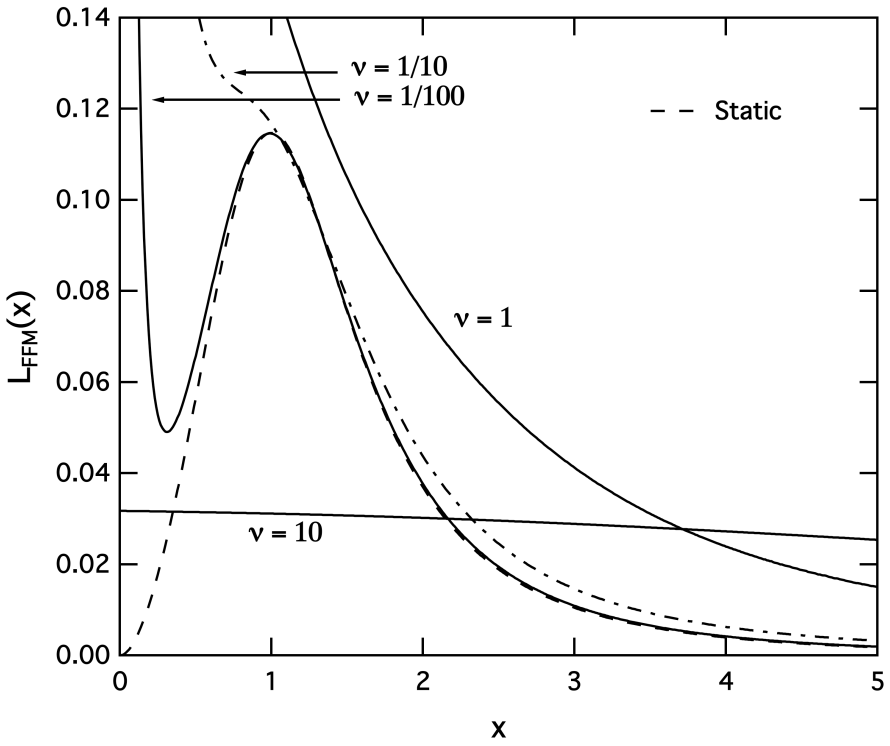

Fig. 1 The static (*dash*) and FFM profiles for the Lyman-α line in dimensionless units for several values of ν labeled in the figure.

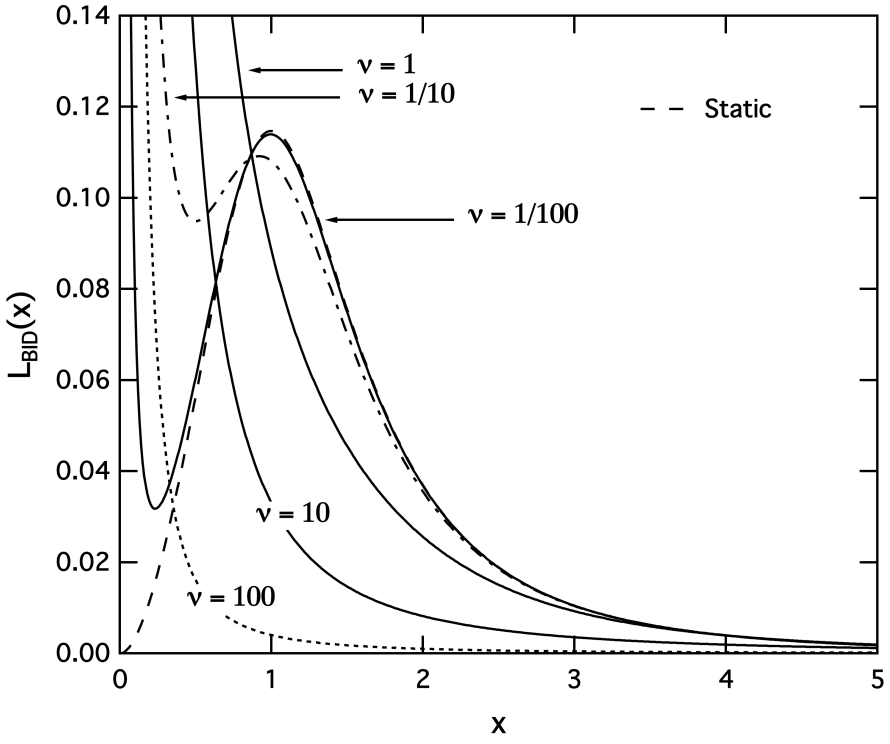

Fig. 2 The static (*dash*) and FFM profiles for the Lyman-α line in dimensionless units for several values of ν labeled in the figure.